Silicon-Based Photonic Crystals

Torsten Geppert[1], Joerge Schilling[2], Ralf Wehrspohn[3], and Ulrich Gösele[1]

[1] Max Planck Institute of Microstructure Physics,
Weinberg 2, 06120 Halle (Saale), Germany
{tgeppert,goesele}@mpi-halle.de
[2] California Institute of Technology,
M.C.136-93 Pasadena CA 91125-3600, USA
schill@caltech.edu
[3] Nanophotonic Materials Group, Department of Physics, Paderborn University,
Warburger Str. 100, 33098 Paderborn, Germany
wehrspohn@physik.uni-paderborn.de

Abstract. We introduce the concept of silicon-based photonic crystals with the main focus on the macroporous silicon material system. photonic crystals are the optical analog to electronic semiconductors. Due to their periodic modulation of the refractive index they exhibit a band-structure for photons propagating in the Photonic crystal. This photonic band structure and in particular the photonic band-gap provide a number of interesting effects for both fundamental research as well as applied physics. These effects include, e.g., forbidden propagation of photons for certain frequencies or a huge reduction of the group velocity. The macroporous silicon material system allows the fabrication of photonic crystals with high dielectric contrast and a variety of patterns as well as defect incorporation using lithographic prestructuring and subsequent photoelectrochemical etching. The etching process will be discussed and experimental results of two-and three-dimensional photonic crystals based on macroporous silicon will be presented and their optical properties will be explored.

1 Introduction

The concept of photonic crystals was introduced to the scientific community in 1987 independently by *Sajeev* [1] and *Yablonovitch* [2]. John's approach was to study the localization of photons in disordered dielectric superlattices while Yablonovitch investigated the inhibited spontaneous emission of an atom within a photonic crystal.

Photonic crystals are the optical analog of electronic semiconductors. In semiconducting materials the electron waves experience scattering at the periodic electrostatic potential provided by the crystal lattice atoms. Due to the interference of these electron-waves the dispersion relation of free electrons $E^{\text{free}}_{\text{electron}}(\boldsymbol{k}) = \hbar\boldsymbol{k}^2$ is replaced by the electronic band-structure which relates the energy E and the quasi-momentum $\boldsymbol{k}$ of the electron.

The potential which photons experience is the refractive index $n = \sqrt{\epsilon}$ of a dielectric medium with dielectric constant ϵ as depicted in Fig. 1. Analogous

L. Pavesi, D. J. Lockwood (Eds.): Silicon Photonics, Topics Appl. Phys. **94**, 295–323 (2004)

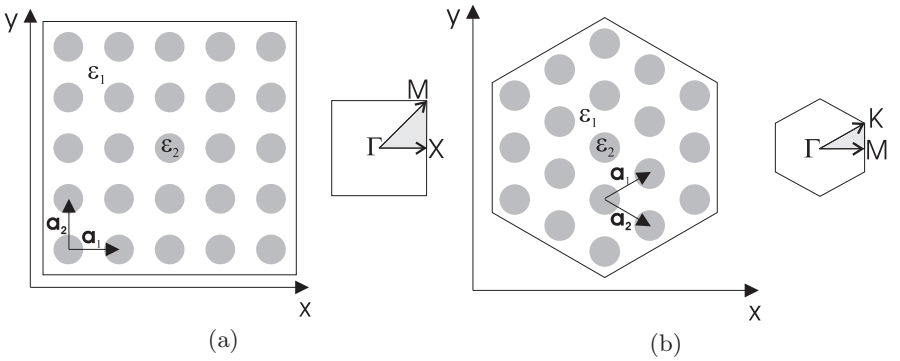

Fig. 1. Arrangement of a material of dielectric constant ϵ_2 within a material of dielectric constant ϵ_1. This could be experimentally realized as, e.g., air pores along the z-direction in bulk Si. (**a**) Square lattice and (**b**) hexagonal lattice. $\overrightarrow{a_1}$ and $\overrightarrow{a_2}$ represent basis vectors of the underlying photonic crystal lattice. The righthand insets depict the corresponding Brillouin zones with points of high symmetry. The shaded region represents the irreducible Brillouin zone

to the electronic case a periodic modulation of this potential leads to the formation of a photonic band-structure which determines the propagation of light within the photonic crystal and eventually also to the formation of a photonic band-gap. Here the photonic band-structure replaces the dispersion relation of photons $\omega = (c/n)|\boldsymbol{k}|$ in a homogenous dielectric with refractive index n and frequency ω along the direction $\boldsymbol{k}$ where c is the speed of light in vacuum. Photons with an energy that lies within the photonic band-gap cannot propagate through the photonic crystal due to the zero density of photonic states in the photonic band-gap.

The band-structure depends on several parameters of which the most important are the symmetry of the modulation of the refractive index, the difference of the dielectric constants of the materials used to achieve the modulation (the so-called dielectric contrast) and the relative prportions of the different materials within the photonic crystal structure. Figure 2 shows the calculated photonic band-structure for a photonic crystal created by photoelectrochemical etching of air pores into bulk Si. This leads to a hexagonal, periodic arrangement of dielectric structures with a very high dielectric contrast of $\Delta\epsilon = \epsilon_{\mathrm{Si}} - \epsilon_{\mathrm{air}} = 11.6 - 1 = 10.6$. Because this photonic crystal has its periodicity in the x-y-plane and is translationally invariant along the z-axis the photonic crystal modes split up into the two independent polarizations TE (transverse electric) and TM (transverse magnetic) with their $\boldsymbol{H}$ and $\boldsymbol{E}$ along the pore axis, respectively. A complete photonic band-gap, i.e., a photonic band-gap for all directions and all polarizations opens up for normalized frequencies $(\omega a)/(2\pi c)$ between 0.377 and 0.389. The width of the complete photonic band-gap which is defined as the ratio of the difference of the maximum and minimum normalized frequencies of the photonic band-gap divided

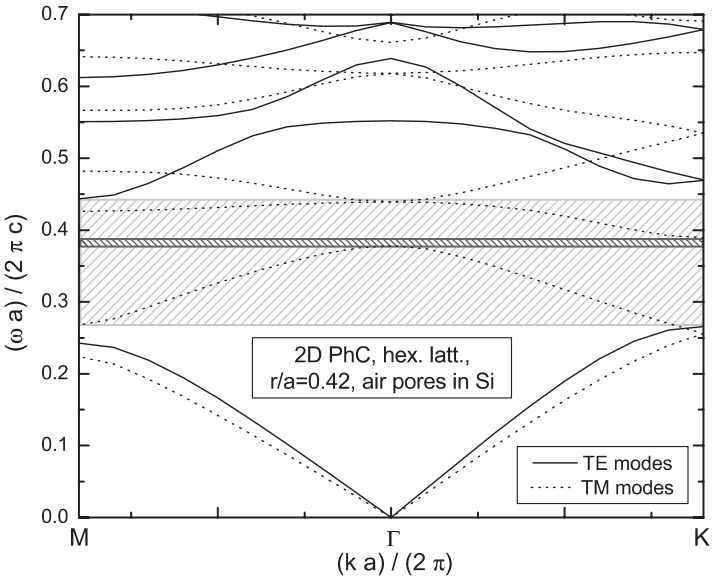

Fig. 2. Calculated photonic band-structure of a hexagonal array of air pores etched into bulk Si. The dielectric constants of the materials are $\epsilon_{\mathrm{Si}} = 11.6$ and $\epsilon_{\mathrm{air}} = 1$. The hatched areas mark the regions of photonic band-gaps for TE (*light grey*) and TM (*dark grey*) polarized modes. There exists a photonic band-gap for both polarizations along both high symmetry directions ΓK and ΓM. But only where these photonic band-gaps overlap a complete photonic band-gap does exist, i.e., a photonic band-gap for all directions and all polarizations. For the calculation the *MIT Photonic Bands* package was used

by the midgap frequency for this structure is about 3%. The TE photonic band-gap is larger than the TM photonic band-gap and the latter one limits the complete photonic band-gap for this structure. The use of the normalized frequency instead of just the conventional angular frequency ω as well as the distinction between TE and TM modes will be explained in Sect. 2 dealing with the theory of photonic crystals.

By changing the above mentioned parameters it is possible to tailor the optical properties of a photonic crystal, e.g., shifting its photonic band-gap to higher or lower frequencies. This possibility to engineer the band-structure offers a large number of opportunities for both fundamental research as well as applications in the field of optoelectronics and photonics.

The lifetime of an excited atom that is placed inside a three-dimensional photonic crystal and which would reach its ground state by the emission of a photon of a frequency that lies within the photonic band-gap should be infinite. This is due to the fact that there are no allowed states for the photon in the photonic band-gap.

For application purposes the photonic band-gap also holds great promises. If, e.g., by the introduction of defects in the photonic crystal lattice, localized states within the photonic band-gap are generated, light with a specific frequency can travel through the photonic crystal without leaking into neighboring modes due to the zero photonic density of states for those neighboring modes. By this method light can be guided not using total internal reflection (TIR) as in conventional optical waveguides but by utilizing a particular property of the photonic crystal structure. Furthermore, based on the photonic band-structure, the group velocity of certain modes travelling in a photonic crystal structure can be strongly reduced which offers a new method for dispersion compensation in photonic circuits.

The above mentioned passive photonic crystal devices can be fabricated reasonably well and their optical properties experimentally verified. But there still remains the challenge to realize active photonic crystal based devices like optical switches or optical transistors which would allow the fabrication of optical processors with very high clock rates and almost no heating problems which limit the performance of today's microelectronic devices.

The practical realization of photonic crystals however is still a challenge for several reasons. The control of light in the photonic crystal is solely based on the periodicity of the photonic crystal's lattice or well controlled deviations thereof, so-called defects. Appropriate means have to be found to guarantee this periodicity during fabrication of a photonic crystal structure. Furthermore, this periodicity has to be ensured on a micrometer scale for the mid-infrared (MIR) down to a nanometer scale for visible (VIS) light.

Approaches to fabricate photonic crystal structures range from self-assembly techniques over interference techniques to the controlled etching of lithographically predefined structures. Self-ordering techniques are relatively inexpensive and easy because no external means are necessary to produce a regular structure. But their major shortcoming consists in the inherent impossibility to incorporate well defined defects such as, e.g., cavities or waveguides. This is however possible using the more expensive and time consuming approaches based on lithography. Table 1 gives a brief overview of some currently used methods for the fabrication of photonic crystals.

Macroporous silicon is a well suited material system for the fabrication of photonic crystals for the near-infrared (NIR) and MIR spectral regions for a number of reasons. Due to its dielectric constant $\epsilon_{\mathrm{Si}} = 11.6$ in the MIR it provides a high dielectric contrast with air and therefore offers the possibility to achieve large photonic band-gaps. Furthermore, Si shows only very little absorption in this spectral region. In addition it is possible to etch highly ordered arrays of macropores into Si with aspect ratios exceeding 100. Using lithographical prestructuring a number of lattice geometries like hexagonal or square lattices can be realized. Furthermore it is also possible to precisely incorporate defects in many shapes using lithographical prestructuring. The lattice constants can be chosen from $a = 500\,\mathrm{nm}$ up to about

Table 1. Overview of different techniques used to fabricate photonic crystals

Material system	Refractive indices n	Dielectric contrast $\Delta\epsilon$	Fabrication principle
air pores in IV semiconductors (Si, Ge)	1, 3.4	10.6	wet and dry etching; self-organiszed or lithographically predefined patterns
air pores in III/V Semiconductors (Ga(in)As, InP ...)	1, 3.4–3.5	10.6–10.9	wet or dry etching after lithographical patterning
air inclusions in polymers (PMMA, photoresist)	1, 1.5	1.25	ordered self assembly of monodisperse spheres after evaporation of solvent; ordered development of photoresist using interference or lithographically defined patterns

$a = 20\,\mu\text{m}$. In addition the variation of the ratio of the pore radius r and the lattice constant a, the so-called r/a-ratio allows the variation of the photonic band-structure by shifting it to higher or lower frequencies. The very small coefficient of thermal expansion ($\alpha = 2.3 \times 10^{-6}\ \text{K}^{-1}$) assures that for moderate temperatures the lattice constant of the photonic crystal remains almost unchanged and therefore the photonic crystal based optical properties of the material are temperature independent. After the etching process the pores can be widened by thermal oxidation of the Si and subsequent etching of the SiO_2 in hydrofluoric acid (HF). Furthermore, due to its dominating role in today's electronics Si is one of the most comprehensively investigated materials.

2 Theory of Photonic Crystals

In this section a brief approach to the theoretical background of photonic crystals is presented. Advanced treatments of photonic crystal theory can, e.g., be found in [3] and [4]. First the relation of Maxwell's equation to photonic crystals is described, followed by brief remarks on how to find solutions for the resulting equations. The subsequent part deals with symmetries, scaling and defects.

2.1 Maxwell's Equations in Periodic Dielectric Media

The propagation of light in dielectric media is governed by the macroscopic Maxwell equations

$$\nabla \times \boldsymbol{D} = \rho \tag{1a}$$

$$\nabla \times \boldsymbol{B} = 0 \tag{1b}$$

$$\nabla \times \boldsymbol{E} = -\frac{\partial \boldsymbol{B}}{\partial t} \tag{1c}$$

$$\nabla \times \boldsymbol{H} = \frac{\partial \boldsymbol{D}}{\partial t} + \boldsymbol{j} \tag{1d}$$

where $\boldsymbol{E}$ and $\boldsymbol{H}$ represent the electric and the magnetic field, $\boldsymbol{D}$ and $\boldsymbol{B}$ the displacement and magnetic induction, $\boldsymbol{\rho}$ and $\boldsymbol{j}$ the free charges and currents and c is the speed of light in vacuum, respectively. Assuming linear, homogenous optical materials we have

$$\boldsymbol{D} = \epsilon_0 \epsilon \boldsymbol{E} \tag{2a}$$

$$\boldsymbol{B} = \mu_0 \mu \boldsymbol{H} \tag{2b}$$

with the magnetic permeability and the dielectric constant μ and ϵ of the material. The corresponding free space values for the magnetic permeability and the dielectric constant are represented by μ_0 and ϵ_0, respectively.

For most of the materials of interest the magnetic permeability μ is close to unity. Furthermore in the following only charge- and current-free media will be treated, i.e., $\boldsymbol{\rho} = \boldsymbol{j} = 0$. Using these simplifications and (2a), (2b) and Maxwell's equations (1c)–(1d) together with the ansatz of harmonic waves

$$\boldsymbol{H}(\boldsymbol{r}, t) = \boldsymbol{H}(\boldsymbol{r}) e^{-i\omega t} \tag{3a}$$

$$\boldsymbol{E}(\boldsymbol{r}, t) = \boldsymbol{E}(\boldsymbol{r}) e^{-i\omega t} \tag{3b}$$

for the magnetic and electric fields, respectively, the time dependence can be separated out and after some algebra the so-called *master equation* for the magnetic field follows:

$$\nabla \times \left(\frac{1}{\epsilon(\boldsymbol{r})} \nabla \times \boldsymbol{H}(\boldsymbol{r}) \right) = \left(\frac{\omega}{c} \right)^2 \boldsymbol{H}(\boldsymbol{r}) \,. \tag{4}$$

Equation (4) determines the distribution of the magnetic field $\boldsymbol{H}(\boldsymbol{r})$ and the corresponding freuqencies ω inside the photonic crystal which is defined by $\epsilon(\boldsymbol{r})$. Furthermore from Maxwell's equations (1a) and (1b) the so-called transversality requirement has to be fulfilled, stating that for a field distribution of the form $\boldsymbol{H}(\boldsymbol{r}) = \boldsymbol{H}_0 e^{i\boldsymbol{k}\times\boldsymbol{r}}$ the relation

$$\boldsymbol{H}_0 \times \boldsymbol{k} = 0 \tag{5}$$

must hold, i.e., the waves are transverse only. From the solution for $\boldsymbol{H}(\boldsymbol{r})$ the electric field distribution can be derived using Maxwell's equations.

2.1.1 Numerical Approaches to Find the Field Distributions

Only for very few $\boldsymbol{\epsilon}(\boldsymbol{r})$ distributions like the very simple case of a homogeneous dielectric medium or the simplest one-dimensional photonic crystal, the Bragg stack or dielectric mirror, it is possible to find analytical solutions for the fields. There are two widely used numerical schemes to calculate the photonic band-structure and field distributions for photonic crystals with more complicated $\epsilon(\boldsymbol{r})$ distributions.

One approach is the Finite-Difference Time-Domain (FDTD) analysis which solves Maxwell's equations in real space in the time domain [5]. FDTD is a general method for numerically solving the time-dependent Maxwell equations in media structured on the order of the wavelength of the light. Therefore it is a well-suited approach to study light propagation in photonic crystals with and without defects. The photonic band-structure can be calculated via a Fourier transformation of the time-dependent FDTD simulation data. The FDTD method can also be used to examine nonlinear and active media. FDTD approaches therefore complement spectral methods used in photonic crystal band-structure calculation described below.

The second widely used method is based on plane wave expansion of the fields $\boldsymbol{H}(\boldsymbol{r})$ and the dielectric distribution $\epsilon(\boldsymbol{r})$. This finally leads to Bloch's theorem, which states that for any kind of periodic potentials the solutions to the master equation are of the form

$$\boldsymbol{H}_{n,\boldsymbol{k}}(\boldsymbol{r}) = e^{i\boldsymbol{k}\times\boldsymbol{r}}\boldsymbol{u}_{n,\boldsymbol{k}}(\boldsymbol{r})\,, \tag{6}$$

where n is the band index, $\boldsymbol{k}$ represents the wave vector and $\boldsymbol{u}_{n,\boldsymbol{k}}(\boldsymbol{r})$ is a function with the periodicity of the photonic crystal lattice, i.e., of the $\epsilon(\boldsymbol{r})$ distribution.

The approach based on plane wave expansion using Bloch's theorem is well suited for defect free photonic crystals. However, because this approach is based on perfect periodicity, it can be used for calculations of defect structures only after utilizing the trick of introducing artificial periodicity using supercells similar to what has been used in disordered semiconductors. As photonic crystals are the optical analogs to electronic semiconductors a lot of knowledge from the field of electronic band-structure calculation can be transferred to the photonic crystal field. However, there are two important differences between electronic and photonic band-structure calculations. In optics the potential, i.e., the $\epsilon(\boldsymbol{r})$ distribution is well known while in solid state physics the potentials of the lattice atoms are unknown and self-consistent approaches have to be used. In addition, neglecting the relatively weak contributions of the vectorial nature of the electron spin, the solutions to the Schrödinger equation, i.e., the electron wave functions, are scalar while the solutions to the master equation (4), namely $\boldsymbol{H}(\boldsymbol{r})$ and $\boldsymbol{E}(\boldsymbol{r})$, are vectorial.

2.2 Symmetry, Scaling and Defects

Defining the Hermitian operator Θ

$$\Theta \boldsymbol{H}(\boldsymbol{r}) = \nabla \times \left(\frac{1}{\epsilon(\boldsymbol{r})} \nabla \times \boldsymbol{H}(\boldsymbol{r}) \right) \tag{7}$$

the master equation takes on the form of an eigenvalue problem $\Theta \boldsymbol{H}(\boldsymbol{r}) = (\omega/c)^2 \boldsymbol{H}(\boldsymbol{r})$ where the frequency ω denotes the eigenvalue. Due to the hermiticity of Θ the eigenvalues ω are real and positive and the eigenfunctions, i.e., the field distributions $\boldsymbol{H}(\boldsymbol{r})$, are orthogonal.

Another important property of Θ is its lineatrity from which follows that any linear superposition $a_1 \boldsymbol{H}_1(\boldsymbol{r}) + a_2 \boldsymbol{H}_2(\boldsymbol{r})$ of solutions $\boldsymbol{H}_1(\boldsymbol{r})$ and $\boldsymbol{H}_2(\boldsymbol{r})$ of the master equation (4) with real numbers a_1 and a_2 is also a solution of (4). From the discrete translational symmetry of $\epsilon(\boldsymbol{r})$ follows the form of the solutions as Bloch functions as described in Sect. 2.1.1. Furthermore it can be shown that the photonic band-structure $\omega(\boldsymbol{k})$ posesses the same symmetry as the photonic crystal's Brillouin zone. As a special and important case of this property it follows that for a photonic crystal having mirror symmetry the solutions of the master equation (4) separate into two classes, one for each field polarization. In Fig. 1 the depicted photonic crystal has mirror symmetry with respect to the x-y-plane. Due to this mirror symmetry the modes separate into TE modes having field components $\boldsymbol{E}_z = \boldsymbol{H}_x = \boldsymbol{H}_y = 0$ and TM modes with field components $\boldsymbol{E}_x = \boldsymbol{E}_y = \boldsymbol{H}_z = 0$ using the coordinate system of Fig. 1.

The inversion symmetry of the dispersion relation $\omega_{-\boldsymbol{k}} = \omega_{\boldsymbol{k}}$ follows from time reversal symmetry $t \rightarrow t' = -t$ of the operator Θ.

Another very useful property of photonic crystals is the scaling law. It states that if the photonic crystal structure is rescaled, i.e.,

$$\epsilon'(\boldsymbol{r}) = \epsilon(\boldsymbol{r}/s) \tag{8}$$

the mode profiles and the frequencies are also rescaled according to

$$\boldsymbol{H'}(\boldsymbol{r}) = \boldsymbol{H}(\boldsymbol{r}/s) \tag{9}$$

$$\omega' = \omega/s \tag{10}$$

where s is the scaling factor. This means that there is no fundamental length scale in photonic crystals. For experiments this property brings great relief, because as mentioned before it is quite hard to fabricate photonic crystals on a micro- or nanometer scale. By using the scaling law one can explore a photonic crystal's band-structure using a macroscopic $\epsilon(\boldsymbol{r})$ with a length scale of a few centimeters, knowing that one only has to rescale the field distributions and frequencies according to the above equations (9) and (10). This scale invariance is also the reason for the usage of the normalized frequency $(\omega a)/(2\pi c)$ instead of the conventionally used angular frequency ω because

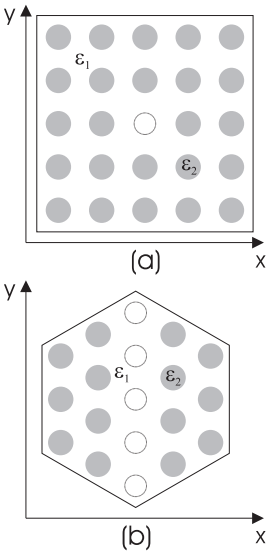

Fig. 3. (**a**) a point defect in a two-dimensional square photonic crystal realized by omitting one air pore and (**b**) a line defect along the ΓK direction in a hexagonal two-dimensional photonic crystal realized by omitting *one* line of pores leading to the name *W*1 defect

the photonic band-structure of, e.g., Fig. 2 holds for any hexagonal photonic crystal with dielectric contrast of $\Delta\epsilon = 10.6$ and $r/a = 0.42$. Rescaling of the photonic crystal's lattice constant a simply shifts the band-structure to higher or lower frequencies. The normalized frequency $(\omega a)/(2\pi c)$ can be rewritten as a/λ from which the wavelength λ can be easily derived from the lattice constant a of the photonic crystal.

As mentioned in the introduction, photonic crystals can be seen as the optical analog to electronic semiconductors. Disturbing the electronic semiconductor host matrix, e.g., by the incorporation of dopant atoms, leads to new electronic states, the so-called acceptor and donor states. Breaking the strict periodicity of the photonic crystal lattice, e.g., by omitting one or several pores as shown in Fig. 3, has as a consequence the formation of new photonic states in the photonic band-structure as depicted in Fig. 4. Introduction of a line defect into the hexagonal photonic crystal leads to several new modes in the photonic band-gap of the bulk crystal.

Figure 3a shows a simple realization of a so-called cavity, while Fig. 3b shows a W1 line defect in a hexagonal lattice along the ΓK direction. Comparison of the TE band-structures of the bulk photonic crystal with undisturbed periodicity and of the photonic crystal with an incorporated W1 waveguide in Fig. 4 clearly reveals some new photonic states in the photonic band-gap which is depicted as the hatched region. Furthermore, the introduction of the W1 waveguide leads to slight shifts of the frequencies of the bulk photonic crystal due to the change in effective refractive index caused by the omitted pores of the waveguide. The frequency of the defect states can also be adjusted by changing, e.g., the radius of the defect pore or by using a W3

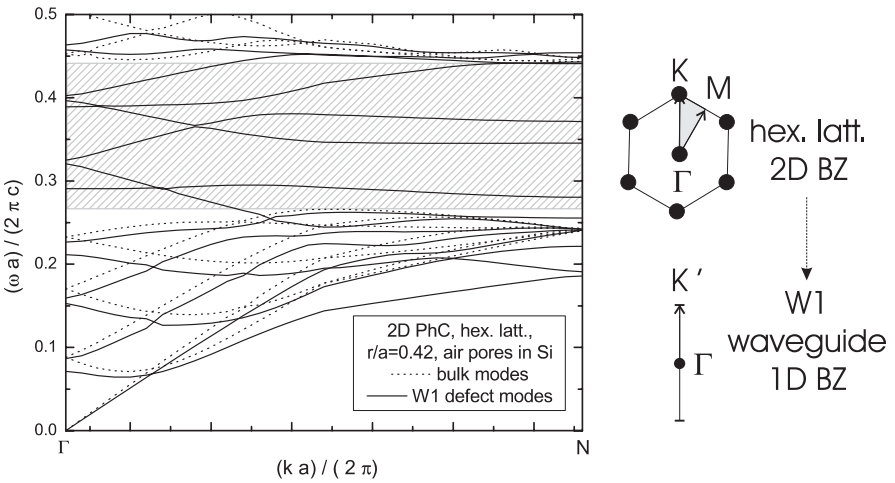

Fig. 4. *Left*: Calculated photonic band-structure for TE modes of a hexagonal array of air pores with $r/a = 0.42$ (*dotted lines*) in bulk Si and of the same structure with an incorporated W1 waveguide along ΓK direction as depicted in Fig. 3b (*full lines*). The hatched region represents the band-gap of the bulk photonic crystal. *Right*: Brillouin zones (BZ) of an undisturbed hexagonal lattice of pores (*top*) and for a W1 waveguide structure (*bottom*)

waveguide with three missing rows of pores instead of only one missing pore row as in the case of the W1 waveguide. For sake of completeness it should be noted that introduction of the waveguide reduces the symmetry from two-dimensional in the bulk photonic crystal to one-dimensional in the photonic crystal with waveguide as shown in the right part of Fig. 4. This has to be taken into account for the photonic band-structure calculation in which the edge of the bulk photonic crystal Brillouin zone K is replaced by the edge of the W1 photonic crystal Brillouin zone K′ [6].

3 Photonic Crystals Based on Silicon

After the short introduction to the theory of photonic crystals in the previous section we will now focus on their experimental realization using Si. In the first part a brief overview of different approaches is given and thereafter we will focus on photoelectrochemically etched macroporous silicon. The etching process will be described. The structure of the photonic crystals is investigated using scanning electron microscopy (SEM). Transmission and reflection measurements are used to characterize the optical properties of the samples. Both, two-dimensional photonic crystals without and with defects will be discussed, followed by consideration of three-dimensional photonic crystals. Regarding poregrowth in Si we will mainly focus on macropore formation in

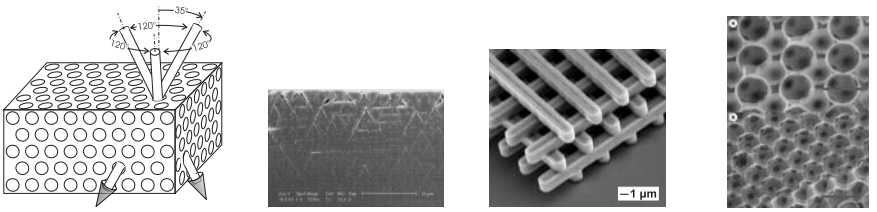

(a) (b) (c) (d)

Fig. 5. (**a**) Yablonovite structure; (**b**) *p*-type macroporous Si Kielovite structure [9]; (**c**) Si Lincoln-Log structure [10]; (**d**) [110] and [111] facets of an Si inverse opal structure [11]

n-type Si. More comprehensive reviews of different pore regimes and pore formation mechanisms in *p*-type and *n*-type Si can be found in [7] and [8].

3.1 Silicon-Based Photonic Crystals – An Overview

Silicon is the dominating material in today's microelectronics and therefore a lot of experience in microstructuring of Si exists. Due to its high dielectric constant $\epsilon = 11.6$ it provides a high dielectric contrast with air. This makes it a promising candidate for photonic crystal fabrication.

From an intuitive point of view one would expect a complete photonic band-gap for a structure for which the interference occurs along all spatial directions for the same wavelength. This means that the Brillouin zone of such a photonic crystal should be sphere-like. A periodic arrangement of dielectric scatterers in a face-centered-cubic (fcc) lattice was therefore initially favored but theoretical calculations showed that even for arbitrarily high dielectric contrast such a structure would not exhibit a complete photonic band-gap. However, the situation changes when a two-atom basis is used resulting in a diamond structure featuring a complete photonic band-gap [12] because the polarization degeneracy of the one-atomic fcc-structure is lifted. A corresponding structure having diamond symmetry and known as *Yablonovite* [13] was the first experimentally realized photonic crystal showing a complete photonic band-gap although in the microwave range. It consists of holes drilled into a dielectric under certain angles as shown in Fig. 5a. It is possible to fabricate a similar structure, the *Kielovite* [9], by etching pores into (111) oriented *p*-type silicon. In contrast to the macropores grown perpendicular to the surface of (100) oriented *n*-type Si focused on later in this article, the macropores in (111) oriented *p*-type silicon can be etched along the ⟨113⟩ crystalline direction as shown in Fig. 5b. The difference consists in the angle of only 29.5° off axis orientation for the Kielovite compared to 35° for the Yablonovite. Calculations by *John* [14] suggest that the Kielovite structure should exhibit a complete photonic band-gap for an appropriate pore diameter.

Another approach to fabricate a three-dimensional photonic crystal is the so-called Lincoln-log structure shown in Fig. 5c as fabricated by Lin and coworkers at *Sandia National Laboratories* [10]. It consists of Si bars stacked on top of each other with subsequent layers arranged orthogonally to one another and the bars in each layer are parallel. Every third layer is shifted by half of the distance between two logs in the first layer. Such a Lincoln-log structure can be fabricated by depositing a layer of SiO_2 which is then structured and trenches are etched. The remaining gap is filled with polycrystalline Si. Repetition of this procedure leads to the desired structure after all the remaining SiO_2 is removed in a last step. This procedure is time consuming due to its layer-by-layer fabrication and therefore the vertical extension of these structures is up to now limited to one or two unit cells [15]. However, the layer-by-layer approach allows relatively easy integration of linear defects.

A technique that manages to get along without complex and costly lithography steps is based on self-organization of colloidal particles. Due to their cubic symmetry such structures can not possess a complete photonic band-gap even for the highest dielectric contrast of the constituent materials. However, the inverted structure does have a complete photonic band-gap. Such structures, as the inverted opal in Fig. 5d, can extend over several hundred unit cells. The structure shown in Fig. 5d was fabricated by infiltrating Si into an artificial opal made up by self-organization of silica spheres. The self-organization of the silica spheres solved in aqueous ethylene glycol was achieved by evaporating the solvent. A sintering step is then used to connect neighboring spheres slightly by a tube like SiO_2 cylinder. Now Si is deposited into the space between the connected spheres. Subsequent removal of the silica results in interconnected air spheres within a Si matrix [11]. The first successful realization of such a structure with a midgap frequency at the telecom window at 1.5 µm had a band-gap of about 5% [11].

In principle all of the above structures can also be used as templates for infiltration of high or low refractive index materials, thereby offering further possibilities of tailoring the band-structure of such a photonic crystal.

3.2 Photonic Crystals Based on Macroporous Silicon

After the brief overview of different fabrication techniques for photonic crystals based on Si in general we will now focus on the special case of the macroporous Si material system.

To produce the required periodic variation of the refractive index in order to create a photonic crystal *Grüning* and *Lehmann* [16, 17] as well as *Lau* and *Parker* [18] proposed the macroporous silicon material system. By a photoelectrochemical etching procedure Si is selectively removed from the bulk material resulting in ordered arrays of macropores. Figure 6 schematically shows the relevant aspects during the etching procedure. Before putting

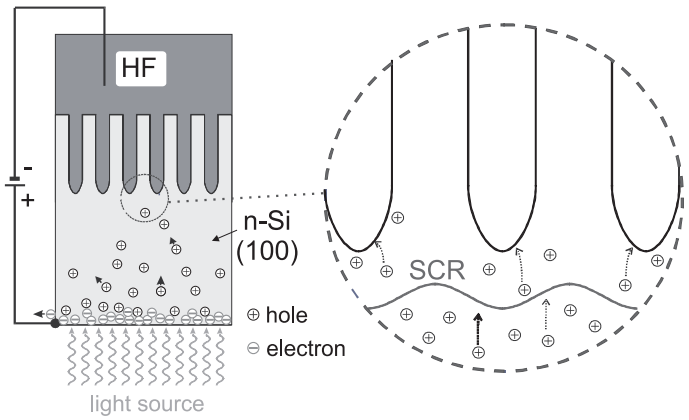

Fig. 6. Schematics of the photoelectrochemical etching process to produce ordered macropores in Si. The backside of the (100) n-Si sample is illuminated to produce holes which diffuse towards the pores where they get focused onto the pore tips by the space charge region (SCR) and promote the dissolution of the Si at the Si/HF interface

the sample into the etching apparatus the surface is lithographically prestructured, e.g., with a square or hexagonal pattern. Using anisotropic KOH etching so-called etch-pits shaped as inverted pyramids are transferred into the Si surface and serve as nucleation sites for the pore growth. Dissolution of Si implies defect electrons, i.e, holes, to be present at the Si/electrolyte interface. Since in the in our experiments used n-type Si holes are minority carriers these holes have to be generated by illuminating the backside of the sample. After photogeneration of the holes they diffuse through the bulk Si towards the pore growth front. The holes are focused onto the pore tips because the space charge region (SCR), resulting from the potential between the Si and the HF electrolyte follows the shape of the pore growth front. If all the parameters like inter pore distance a, potential U and doping of the n-Si are correctly chosen, all holes reaching the pore growth front are focused onto the pore tips where they lead to the dissolution of Si and none of them enter the Si walls separating adjacent pores, thereby passivating the Si walls against dissolution. Increasing or decreasing the intensity of the light source leads to a corresponding change in the number of available holes for the dissolution of Si. By this mechanism it is therefore possible to control the pore diameter. The porosity $p = A_{\text{pore}}/A_{\text{sample}}$ of a macroporous Si photonic crystal is defined as the ratio of the pore area A_{pore} and the total sample area A_{sample}. For a certain current density j_{PS} across the Si/HF interface all of the Si gets dissolved. This is the so called electropolishing regime. According to Lehmann's pore growth model there is a current density $j_{\text{pore}} = j_{\text{PS}}$ across the bottom of each pore during pore growth while there is no current flow across the pore wall/HF interface. Defining an average current density

$j = I/A_{\text{sample}}$ across the sample where I describes the total current and defining the current density across the pores $j_{\text{pore}} = I/A_{\text{pore}}$ and using the above relations the porosity can also be written as $p = A_{\text{pore}}/A_{\text{sample}} = j/j_{\text{PS}}$. The current density j_{PS} can be calculated using the relation

$$j_{\text{PS}} = 3300 \frac{\text{A}}{\text{cm}^2} c_{\text{HF}}^{3/2} e^{\frac{-0.345\ \text{eV}}{k_{\text{B}} T}} \tag{11}$$

where c_{HF} is the concentration of HF in weight percent, k Boltzmann's constant and T the absolute temperature in kelvin. The numbers in (11) are empirically determined parameters. Besides (11) for stable macropore growth the further condition $d_{\text{pore wall}} \approx 2x_{\text{SCR}}$ has to be fulfilled stating that the thickness of the remaining pore walls $d_{\text{pore wall}}$ should be about twice as thick as the extension x_{SCR} of the space charge region. The latter one is determined by

$$x_{\text{SCR}} = \sqrt{\frac{2\epsilon_{\text{Si}}\epsilon_0(V - \phi_0)}{eN_{\text{D}}}} \tag{12}$$

with the dielectric constant of Si being ϵ_{Si}, and the free space permittivity ϵ_0, the fundamental charge $e = 1.69\ \times 10^{-19}$ C and the concentration of dopant atoms N_{D}. ϕ_0 describes the curvature of the bands at the Schottky-contact like Si/HF interface in equilibrium and V is the applied external voltage.

Based on these equations conditions can be chosen to allow for the growth of macropores in n-Si. Details on the electrochemical etching of Si and pore formation can be found in [8, 19, 20].

3.3 2-dimensional Photonic Crystals

In this section two-dimensional photonic crystals based on macroporous silicon will be discussed. Using the previously described photoelectrochemical etching procedure it is possible to obtain pores with aspect ratios clearly exceeding 100. Due to this high aspect ratio these photonic crystals can be seen as almost ideal, i.e., infinitely high, two-dimensional photonic crystals. The lattice constant of the photonic crystal can be varied from 500 nm up to about 20 µm. First bulk photonic crystals will be discussed followed by a treatment of defect structures introduced into two-dimensional photonic crystals.

3.3.1 Bulk 2-Dimensional Photonic Crystals

The structural quality of macropores etched into a Si wafer can be judged by cleaving the sample and examining the cleaving edge using SEM. The Moiré pattern in this printed version underlines the almost perfect straightness of the pores. Figure 7a shows the cleaving edge of hexagonally arranged macropores with a lattice constant of $a = 700$ nm. The aspect ratio of these pores

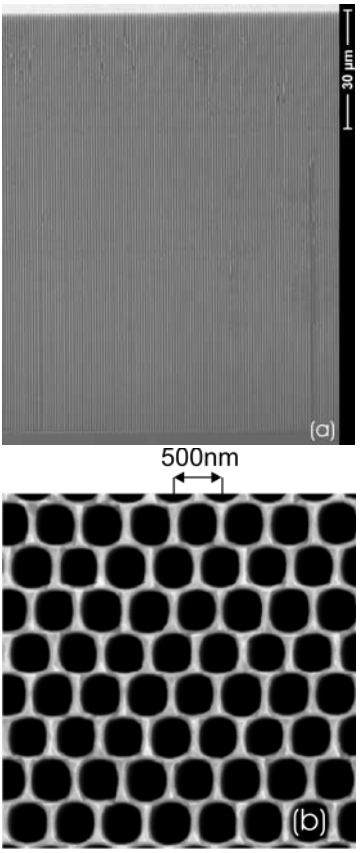

Fig. 7. SEM-image of (**a**) the cleaving edge of a two-dimensional hexagonal lattice of macropores in Si with a lattice constant of $a = 700\,\text{nm}$ (courtesy of S. Schweizer). The pores are straight and parallel providing the required strict periodicity for a photonic crystal. (**b**) Topview of a hexagonal pore array in Si with a lattice constant of $a = 500\,\text{nm}$

is about 100 allowing to treat this photonic crystal as two-dimensional. The pores are straight and parallel providing the strict periodicity of the dielectric materials Si and air needed for a photonic crystal. Figure 7b shows the topview of a sample with a hexagonal lattice of air pores in Si with a lattice constant of $a = 500\,\text{nm}$.

While SEM investigations give an impression of the structural quality of the etched samples they are not sufficient to judge the sample's photonic properties. For this purpose transmission and reflection measurements were performed. In Fig. 8 the calculated reflectivity on the left can be compared to the measured reflectivity in the center diagram and to the photonic bandstructure on the right for a photonic crystal consisting of hexagonally arranged air pores in Si with a lattice constant of $a = 500\,\text{nm}$ and $r/a = 0.425$. The upper part shows the results for TE modes and the lower part for TM modes along the ΓM direction. The dashed lines in the photonic band-structure of Fig. 8 represent so-called noncoupling bands. The electric field along the pore axis $\boldsymbol{E}_z$ of a TM polarized plane wave approaching the photonic

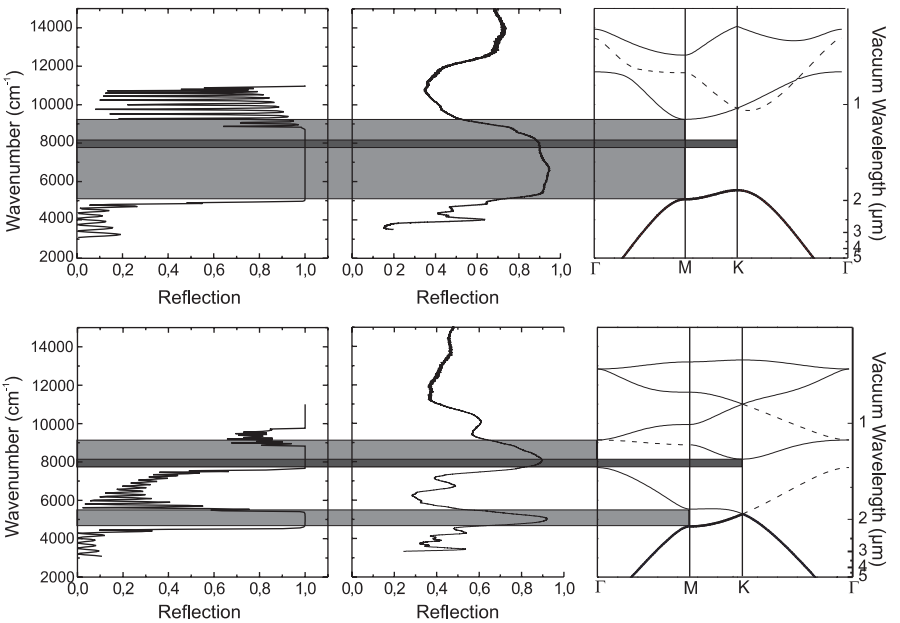

Fig. 8. Reflection of a two-dimensional photonic crystal of hexagonally arranged air-pores with $r/a = 0.425$ in Si along the ΓM direction. *Top*: TE modes, *Bottom*: TM modes. *Left*: Calculation for a finite photonic crystal with 8 pore rows. *Center*: Measurement of a semi-infinite photonic crystal. *Right*: photonic band-structure for comparison. The *dark grey* region represents the complete photonic band-gap

crystal is symmetric with respect to a plane containing the z-axis and the vector of the incoming plane wave. Such a plane wave can only couple to photonic crystal modes if they have the same symmetry.

This is e.g., the case for the second TM band for hexagonally arranged air pores in Si, as can be seen from the upper part of Fig. 9. The lower part of Fig. 9 shows the $\boldsymbol{E}_z$ field intensity for the third TM band which reveals antisymmetry with respect to the previously defined plane. Therefore a plane wave cannot couple to this photonic crystal mode leading to a high reflectivity in the corresponding frequency range although there is no real photonic band-gap. Furthermore, for both polarizations the reflectivity is very high in the photonic band-gap regions. The measurements also agree well with the calculated reflection of a finite photonic crystal structure with 8 pore rows based on a two-dimensional transfer-matrix code using the *Translight* software [21].

Band-gap Tuning and Switching One of the advantages of the macroporous Si/air material system for photonic crystals is that the band-structure can be easily shifted by simply changing the r/a-ratio. For a fixed lattice constant a the porosity p and with it the pore radius r is determined by the

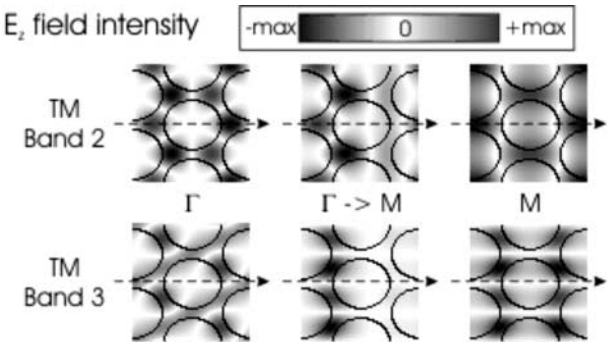

Fig. 9. Field intensity of $\boldsymbol{E}_z$ for the second and third TM bands at the Γ and M points, respectively (*left and right images*) and for $|\boldsymbol{k}| = 1/2\Gamma\mathrm{M}$ (*center image*) along the ΓM direction for a hexagonal photonic crystal of air pores in Si. The dashed arrows mark the ΓM direction

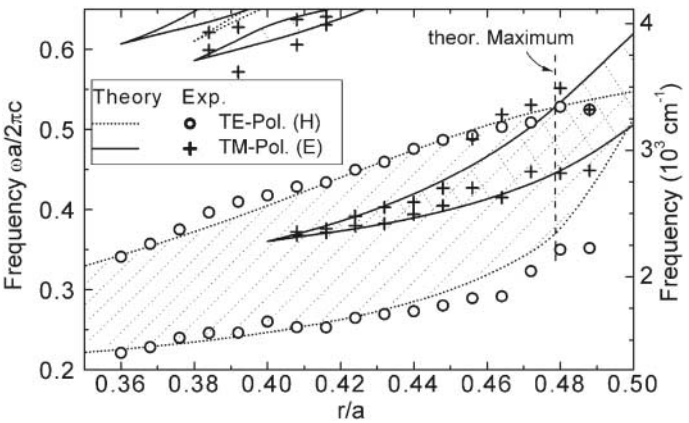

Fig. 10. Theoretical (*lines*) and experimentally verified (*symbols*) position of the TE and TM bandedges depending on the r/a-ratio for a two-dimensional photonic crystal consisting of air pores in Si [23]

current during the etching process. Therefore, it is possible to shift the photonic band-gap by keeping a constant. Figure 10 shows the gapmap, i.e., the bandedges of TE and TM polarized modes for hexagonally arranged air pores in Si depending on a certain parameter as which the r/a-ratio was chosen in this case. The lines represent the results of calculations based on a plane wave expansion method [22] and the symbols are experimentally determined values. Only for the largest r/a-ratios, i.e., the highest porosities, there is a slight discrepancy between theory and experiment. These are due to difficulties in preparing and handling such structures. Hexagonally arranged air pores in Si have a maximum complete photonic band-gap of about 16% for a r/a-ratio of 0.47.

As mentioned in the preceding sections the dielectric contrast as well as the lattice constant and the geometry have a strong influence on the band-structure of a photonic crystal and, consequently, on the position of the photonic band-gap.

A change of one of these parameters will shift the photonic band-gap and allows the realization of an optical switch that blocks light of a certain frequency for one set of parameters while allowing transmission for the changed parameters. A change of the symmetry and the lattice constant could be realized by mechanically stretching or compressing the sample. In the case of a photonic crystal based on macroporous silicon this is not favorable since silicon is a hard and brittle material. Changes of the lattice constant by thermal expansion of the Si are also not practicable due to the very small coefficient of expansion $\alpha = 2.3 \times 10^{-6}\,\mathrm{K}^{-1}$ of Si.

However the dielectric contrast can easily be varied by filling liquid crystals into the macropores. Depending on temperature they are either randomly oriented at 59 °C or higher temperatures or the are in their nematic phase at room temperature, where they are oriented parallel to the pore axis [27]. By this method it was possible to achieve a shift of 70 nm for the low-frequency bandedge of hexagonal macropores with $a = 1.58\,\mu\mathrm{m}$ and a photonic band-gap in the frequency range of 4.4 µm to 6 µm. While this method allows for fine tuning of the photonic band-structure, e.g., to compensate for fabrication tolerances, it is not suitable for high speed switching applications because it takes several microseconds for the liquid crystals to undergo the necessary phase change from their nematic ordering into random orientation.

Another possibility to change the dielectric contrast is to vary the dielectric constant of the Si itself. This can be achieved by the creation of carriers by illumination of the sample leading to a change of the dielectric constant $\epsilon(\omega) = \epsilon_{\mathrm{Si}} - \omega_{\mathrm{P}}/\omega^2$ where ϵ_{Si} is the dielectric constant of Si in the absence of free carriers and ω_{P} represents the plasma frequency in the Drude model $\omega_{\mathrm{P}} = (Ne^2)/(\epsilon_0 m^*)$ with the reduced effective mass $1/m^* = 1/m_e^* + 1/m_h^*$, the number N of generated free carriers and the elementary charge $e = 1.69 \times 10^{-19}$ C. The photonic band-structure and the expected shift of the bandedge depending on plasma frequency is shown in Fig. 11. By this method a 29 nm shift of the bandedge at 1910 nm with free carriers was achieved [28, 29]. The turn on time of about 400 fs of this optically induced bandedge shift is rather short and promising for high speed switching. Since Si is an indirect semiconductor the turn off time is on the order of several nanoseconds limiting the switching speed. Theoretical considerations, however, suggest that it should be possible to reduce the switch off time to about 10 ps using defect induced de-excitation via surface states or impurity atoms incorporated into the Si.

The transmission through an ideal photonic crystal, i.e., an infinitely extended, perfectly periodic structure $\epsilon(\boldsymbol{r})$, is zero for frequencies within its band-gap. Experimentally fabricated photonic crystals however are by na-

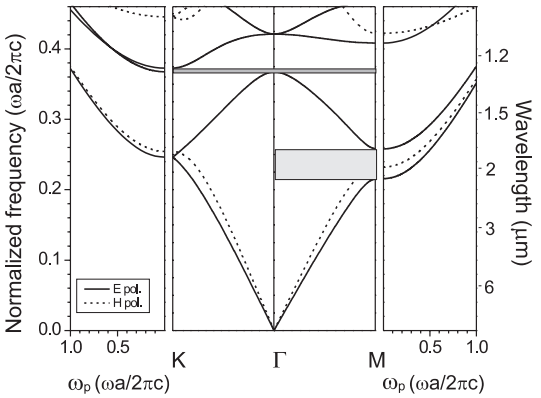

Fig. 11. *Center*: Photonic band-structure of a two-dimensional hexagonal photonic crystal of macroporous Si with $r/a = 0.41$. *Left* and *right*: Changes of the photonic band-gap depending on plasma frequency ω_p at M and K points, respectively [26]

ture finite objects. From this point of view it is desirable to investigate how extended a photonic crystal has to be before light starts to feel the photonic band-gap and cannot travel through the photonic crystal anymore. For this purpose structures consisting of only a few pore rows were prepared. After the standard fabrication of an ordered macropore array by photoelectrochemical etching of Si this photonic crystal was further structured. First the pore walls were passivated by a thermal oxide and a chemical vapor deposited (CVD) nitride. Then an aluminum layer was deposited onto the macropore array and structured by standard photo-lithography. Although the feature size in this step was on the order of 10 μm, the alignment relative to the pores and the precision of these structures was better than 1 μm. In the aluminum mask a window was opened and the passivating oxide and the nitride were removed by chemical etching. The porous Si in the regions without passivating oxide was etched in a subsequent isotropic plasma etching process resulting in structures like the one shown in Fig. 12. Details can be found in [30] and [31]. The resulting structure consisted of only a single pore row along ΓK direction as depicted in the lower right inset in Fig. 12. The lines in Fig. 12 represent the calculated transmission based on an extended plane wave approach [4,31] and the symbols show the results of measurements at structures like the one shown in the lower right inset through 1, 2, 3 and 4 pore rows, respectively. The attenuation of the transmitted signal increases with increasing number of pore rows with a rate of about 10 dB per pore row [24]. Such a signal attenuation by a constant factor per pore row is typical for a evanescent, i.e., exponentially decaying field. These results show that already for rather finite photonic crystals consisting of only a few pore rows practically useful effects are obtained.

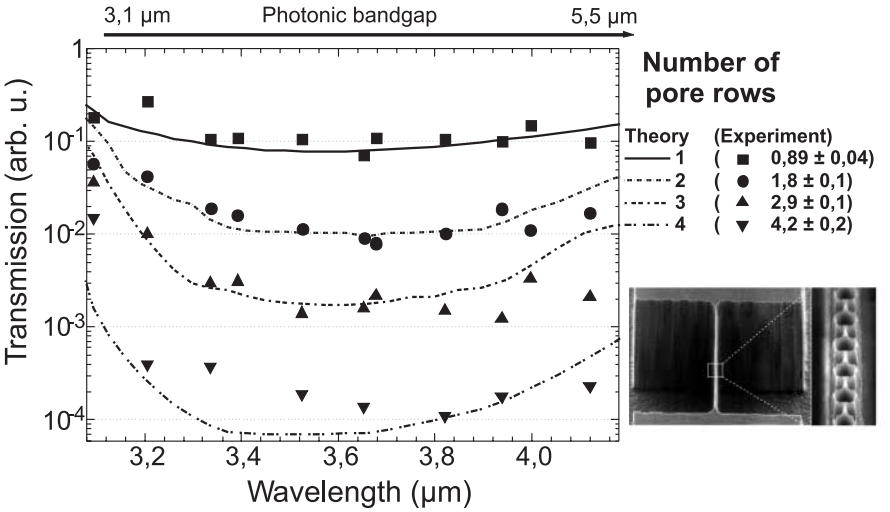

Fig. 12. Calculated (*lines*) and measured (*symbols*) transmission through a few pore rows along ΓK direction. The *lower right inset* shows an SEM picture of the structure [23, 24, 25]

3.3.2 Defects in 2-Dimensional Photonic Crystals

While the bulk photonic crystals treated in the previous section reveal a lot of basic physics it is necessary to implement some functionality for actual applications. This is similar to electronic semiconductors which deploy their full potential and possibilities only after doping which introduces new electronic states in the band-structure. In the case of photonic semiconductors functionality in form of new photonic states is achieved by disturbing the strict periodicity of the underlying crystal lattice by omitting some pores as previously shown in Fig. 3. For macroporous Si defect structures are defined during the lithography step which gives considerable freedom in designing photonic crystals with incorporated defects. The simplest kind of defect is given by a single missing pore as depicted in Fig. 13a. This leads to a new state in the photonic band-gap whose field energy is concentrated in and around this cavity. Omitting subsequent neighboring pores as shown in Fig. 13b–d creates waveguides within the photonic crystal. Although they look similar to conventional waveguides made of bulk Si embedded within a material with lower refractive index and using total internal reflection (TIR) for the guiding the photonic crystal waveguide is based on a fundamentally different waveguiding mechanism. Introducing of a defect leads to the formation of new photonic states within the photonic band-gap. Above and below those defect-induced modes the photonic DOS is zero. As a consequence light travelling in the photonic crystal using the defect modes cannot leak away into neighboring modes and, therefore, ideally the loss is zero. However, the confinement is

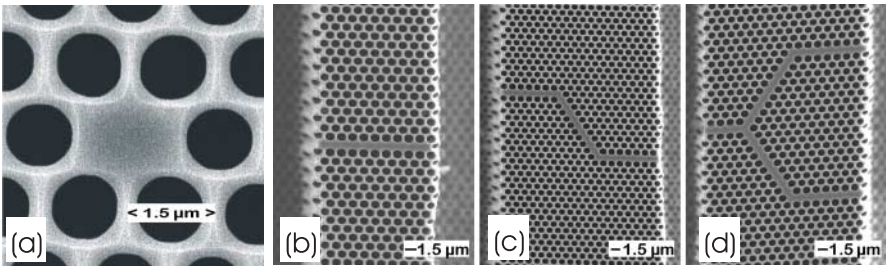

Fig. 13. SEM micrographs of defect structures in a hexagonal lattice of air pores in Si (**a**) a point defect or *cavity* (**b**) and (**c**) straight and bent linear defects and (**d**) Y-branch. Realized by omitting adjacent pores in the otherwise strictly periodic lattice

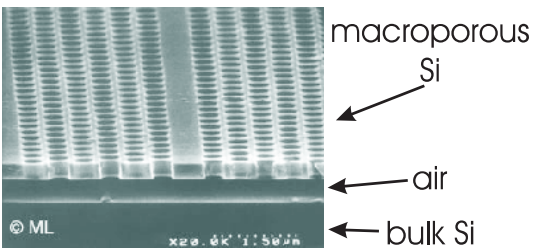

Fig. 14. *Airbridge* structure: macropores etched into Si prepared as a membrane embedded within air [32]

very high only in the plane providing the periodic modulation of the refractive index, i.e., in the x-y-plane, the plane perpendicular to the pore axis. Along the z direction there is no photonic crystal based confinement. By using membrane structures as shown in Fig. 14 consisting of macropore arrays with air or SiO_2 above and below the pores would allow to provide at least partial light confinement along the z direction by TIR.

A closer look onto the SEM micrographs in Fig. 13 reveals that the pores next to defects are somewhat larger than the other pores farther away from the defects because the pores surrounding the defect collect more charge carriers. This effect can be minimized by etching pores with a smaller diameter than the finally desired one and widening of the pores by subsequent thermal oxidation and HF etching of the SiO_2.

After the fabrication of a Si macropore array additional structure can be added. In Fig. 15 a linear defect incorporated into a thin catwalk consisting of 13 pore rows is shown in a zoom series starting from a global overview towards the defect. The high quality of the structure with its high aspect ratio of the catwalk as well as its flat edge are observable. Thinning the catwalk further allows to measure the transmission of single pore rows as shown in Fig. 12.

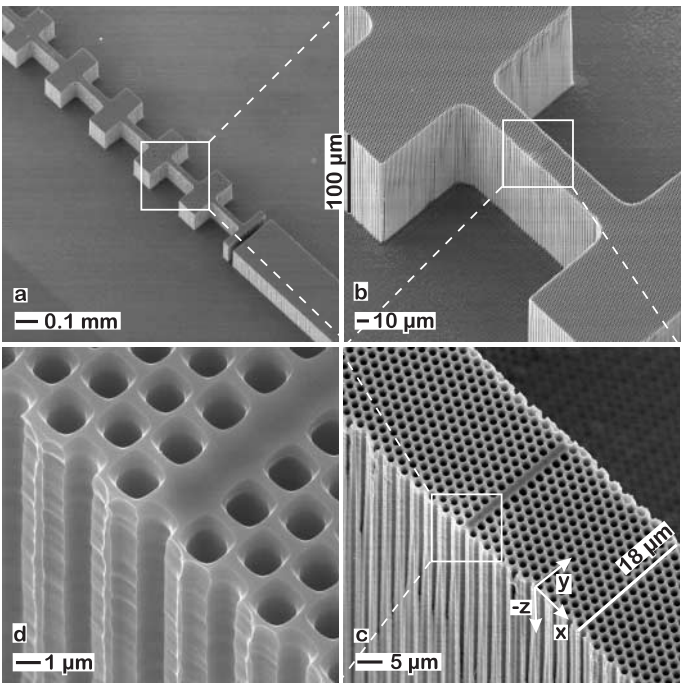

Fig. 15. After photoelectrochemically etching of the Si the macropore array was further structured by subsequent lithographical and wet and dry etching processes. The SEM picture series shows a zoom into the structure finally revealing the high quality line defect incorporated into the thin part of the catwalk [33]

3.4 3-Dimensional Photonic Crystals

Photonic crystal effects only appear in directions where the refractive index changes periodically. This was true for the two-dimensional photonic crystals treated in the previous section in the x-y plane, but not along the z direction. In this section photonic crystals based on macroporous Si will be reviewed whose refractive index is also periodically modulated along the z direction offering the possibility to create three-dimensional photonic crystals.

3.4.1 Bulk 3-Dimensional Photonic Crystals

The diameter of a pore etched into Si depends on the etch current. This current can be controlled by changing the backside illumination intensity which generates the holes necessary for the dissolution of the Si at the pore tip. If the illumination intensity is varied during pore growth the pore diameter will vary correspondingly as is shown in Fig. 16. By this method a nice periodic change in the pore diameter along the growth direction and with it of the refractive index can be achieved. The pore diameter modulation, however, does

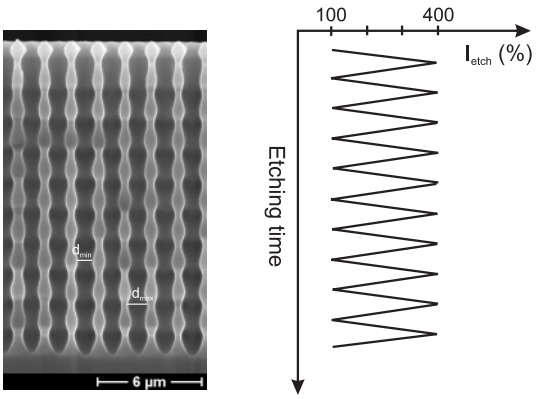

Fig. 16. Variation of the pore diameter along the pore axis is achieved by varying the etch current by changing the illumination intensity. *Left*: Cross-sectional SEM picture of the cleaved sample. *Right*: Schematic diagram of etch current vs. time [29]

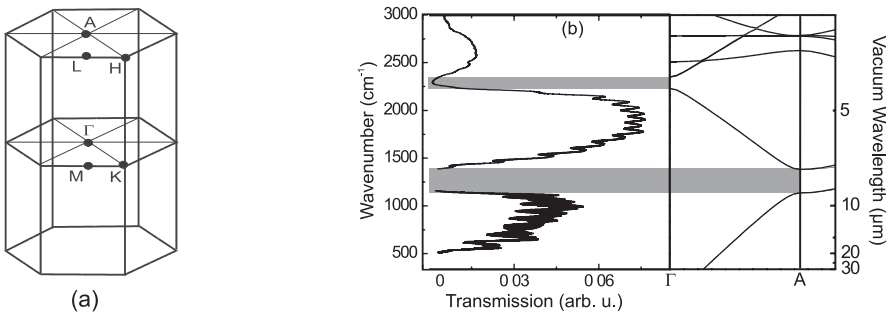

Fig. 17. (**a**) Brillouin zone of a three-dimensional photonic crystal with high symmetry points. (**b**) Transmission along the ΓA direction of a three-dimensional macroporous Si photonic crystal. *Left*: Measured Transmission, *Right*: Photonic band-structure along ΓA. The lattice constant of the hexagonal lattice in the x-y-plane is 1.5 µm. Along the z-axis 15 modulation periods were realized with a length of $l_z = 2\,\mu\text{m}$

not exactly follow the etch current modulation [34]. While the current profile exhibits sharp features the corresponding pore profiles show soft edges. The pore profiles are smeared out. This is due to limitations of the theoretical model on which the current profile is based. If the illumination and with it the free carrier concentration is varied too sudden or too strong the etching mechanism at the pore tip changes leading to the observed deviation of the etched pore shape from the designed profile [29]. Detailed studies on how the current profile has to be chosen to produce desired sharp changes of the pore radius are currently underway.

The Brillouin zone of the three-dimensional photonic crystal is depicted in Fig. 17a. In the x-y-plane it maintains the hexagonal symmetry of the

two-dimensional photonic crystal and gets extended along the z direction due to the introduced periodicity l_z of the pore diameter modulation. To observe the photonic crystal effects caused by this periodic modulation of the refractive index along the z-axis the transmission along the ΓA direction, i.e., along the pores, was measured. The center panel of Fig. 17 shows the measured transmission spectrum of a photonic crystal consisting of air pores in Si with hexagonal lattice constant of 1.5 µm in the x-y-plane and 15 modulations of the pore diameter with a period length of $l_z = 2\,\mu\text{m}$ along the z-axis. The two lowest band-gaps are clearly observed and agree well with the calculated band-structure given in the right panel of Fig. 17b. While in the two-dimensional photonic crystal *every* plane perpendicular to the pore axis was a mirror plane this is no longer true in the three-dimensional photonic crystal. Therefore the modes do no longer separate into TE and TM polarization.

Reduction of the Group Velocity In the case of electronic semiconductors the slope of the band-structure $\partial E_n(\boldsymbol{k})/\partial \boldsymbol{k}$ can in a semiclassical approximation be interpreted as $\hbar$ times the velocity $\boldsymbol{v}_n(\boldsymbol{k})$ of an electron in a definite Bloch level $\Psi_n(\boldsymbol{k})$ with energy $E_n(\boldsymbol{k})$ [35]. In a photonic crystal the slope of the band-structure represents the group velocity $\boldsymbol{v}_n(\boldsymbol{k})$ of light with frequency ω travelling along the direction $\boldsymbol{k}$ in the n-th band

$$\frac{\partial \omega_n(\boldsymbol{k})}{\partial \boldsymbol{k}} = \boldsymbol{v}_n(\boldsymbol{k}) \,. \tag{13}$$

In a linear approximation the inverse slope $(\partial \omega_n(\boldsymbol{k})/\partial \boldsymbol{k})^{-1} = n_{\text{eff}} = c/\boldsymbol{v}_n(\boldsymbol{k})$ can be interpreted as the effective refractive index n_{eff} for that particular frequency. As a consequence flat bands lead to a low group velocity in a photonic crystal.

Experimentally the group velocity $\boldsymbol{v}_n(\boldsymbol{k})$ can be determined from the frequency difference $\Delta\omega_{\max}$ of the Fabry–Perot transmission maxima and the pore depth d_{pore} together with (13). In $\boldsymbol{k}$-space the difference between adjacent transmission maxima $\Delta\omega_{\max}$ is given by $\Delta\boldsymbol{k}_{\max} = \pi/d_{\text{pore}}$. This leads to

$$\boldsymbol{v}_n(\boldsymbol{k}) = \frac{\partial \omega_n(\boldsymbol{k})}{\partial \boldsymbol{k}} \approx \frac{\Delta\omega_{\max}}{\Delta\boldsymbol{k}_{\max}} \tag{14}$$

from which the group velocity can experimentally be determined using the above difference quotient as approximation for the differential quotient in (14). Using such a three-dimensional photonic crystal based on macroporous silicon a reduction of the maximum group velocity to about 30%–40% of the vacuum speed of light c_0 is achieved for the second band in Fig. 17b as shown in Fig. 18 [36]. The lines represent the calculated group velocity derived from the band-structure of the first two bands in Fig. 17b and polarization of the $\boldsymbol{E}$ field along ΓM direction while the symbols are the experimentally obtained

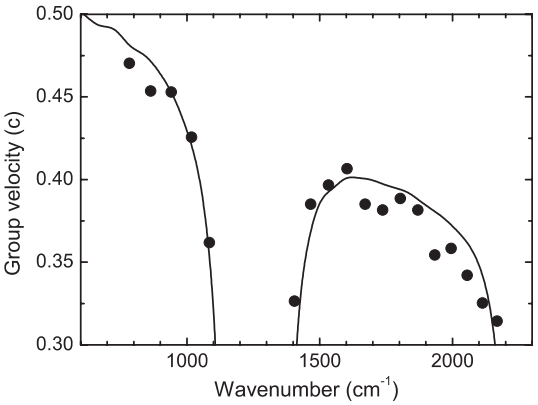

Fig. 18. Group velocity $\boldsymbol{v}_g$ along ΓA direction for the structure in Fig. 17b. The black line is the derivative of the band-structure, the *open symbols* represent the experimentally determined values using the Fabry–Perot resonances in Fig. 17b and (14)

values. It has to be taken into account that simply taking the derivative of, e.g., the second band, in the band-structure in Fig. 17b yields negative values for $\boldsymbol{v}_g$ which makes physically no sense. But this is simply due to the fact that the reduced zone scheme was used in Fig. 17b where the second band seems to have negative slope. In the extended zone scheme the band would have positive slope at every k-point and a physically meaningful positive group velocity would be the result. As mentioned above a flat band corresponds to a high effective refractive index. This in return leads to a high reflection R of incoming light following from the well known equation $R(0°) = \{(n_1 - n_2)/(n_1 + n_2)\}^2$ describing the amount of reflected light R for incidence perpendicular to a dielectric surface in a classical approximation. For this reason it is not possible to experimentally probe the regions of photonic bands with zero slope by transmission.

3.4.2 Defects in 3-Dimensional Photonic Crystals

As shown in Sect. 3.3.2 defects in the x-y-plane in two-dimensional photonic crystals are defined via lithography. As defects are simply well behaved deviations of a photonic crystal's periodicity a defect layer in a three-dimensional macroporous Si photonic crystal can be realized by a current profile like the one shown in Fig. 19a. Leaving the current unchanged for a certain time and thereby keeping the pore radius constant leads to a defect layer within a three-dimensional photonic crystal. An experimental realization of such a structure is shown in Fig. 19b. Experimental results concerning the introduced defect states in the band-structure and their modelling can be found in the thesis of *Schilling* [29] and will be published soon.

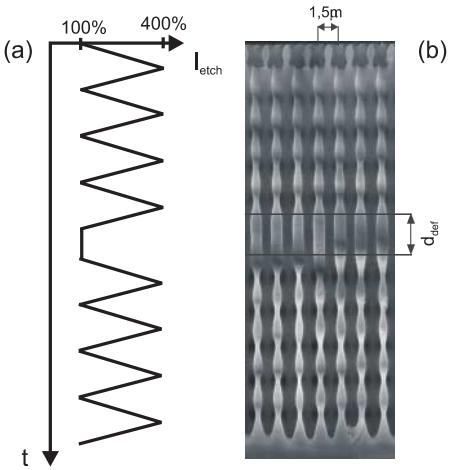

Fig. 19. Defect layer in a three-dimensional photonic crystal based on macroporous Si. (**a**) Schematic representation of the current profile used for the creation of the defect layer within the three-dimensional photonic crystal. (**b**) Cross-sectional SEM picture of the cleaved sample of an etched structure with 5 modulations of the pore diameter above and below the defect layer. The vertical extension of the defect is $d_{\mathrm{def}} = 2.12\,\mu\mathrm{m}$

4 Conclusion and Outlook

The concept of photonic crystals was introduced and a brief introduction to the underlying theory was given. Fabrication methods for Si based photonic crystals including self-organization as well as lithographical approaches were described with special focus to macroporous Si. The latter allows the realization of two-and three-dimensional extended photonic crystals by photoelectrochemical etching of Si in HF. These structures feature ordered pore arrays with high aspect ratios exceeding 100 and provide high dielectric contrast. A variety of macropore patterns like square or hexagonal arrangement can easily be chosen by lithography. Furthermore the lattice constant can be chosen over a wide range from 500 nm up to about 20 µm. This together with the appropriate choice of the r/a ratio allows the fabrication of photonic crystals for the NIR to MIR spectral range. In two-dimensional macroporous Si photonic crystals defects can be incorporated during the lithography process while in three-dimensional structures defects can be incorporated during the photoelectrochemical etching. Macroporous Si pore arrays can also serve as templates which can be filled with, e.g., liquid crystals, to tune the photonic properties such as the position of the photonic band-gap. The basic properties of photonic crystals such as the photonic band-gap, defect states and the reduction of group velocity were experimentally verified with these structures.

Future work includes a better understanding of the photoelectrochemical etching process and application of this knowledge to the fabrication of a three-dimensional photonic crystal with a complete photonic band-gap [37]. For the realization of compact gas sensing devices we plan to use the reduced group velocity to enhance the absorption in two-dimensional photonic crystals [38]. To ensure efficient coupling in spite of the high refractive index and with it

the high back reflection of incident light tapered structures will be fabricated and their efficiency evaluated.

Acknowledgements

The authors are gratefull to S. Schweizer, F. Müller, R. Hillebrand, A. Birner, C. Jamois, K. Busch, S. Leonard and H.M. van Driel for theoretical and experimental contributions. Funding by DFG within SPP1113 is gratefully acknowledged.

References

1. S. John: Phys. Rev. Lett. **58**, 2486 (1987)
2. E. Yablonovitch: Phys. Rev. Lett. **58**, 2059 (1987)
3. J. D. Joannopoulos, R. D. Meade, J. N. Winn: *Photonic Crystals: Molding the Flow of Light* (Princeton University Press 1995)
4. K. Sakoda: *Optical Properties of Photonic Crystals* (Springer, Berlin, Heidelberg 2001)
5. O. Hess, C. Hermann, A. Klaedtke: Phys. Stat. Sol. A **197**, 605 (2003)
6. S. G. Johnson, P. R. Villeneuve, S. Fan, J. D. Joannopoulos: Phys. Rev. B **62**, 8212 (2000)
7. P. Allongue: INSPEC Data Series (1997)
8. V. Lehmann: *Electrochemistry of Silicon* (Wiley-VCH, Weinheim 2002)
9. M. Christophersen, J. Carstensen, A. Feuerhake, H. Föll: Mater. Sci. Eng. B. **69**, 194 (2000)
10. S. Y. Lin, J. G. Fleming, D. L. Hetherington, B. K. Smith, R. Biswas, K. M. Ho, M. M. Sigalas, W. Zubytzki, S. R. Kurtz, J. Bur: Nature **394**, 251 (1998)
11. A. Blanco, E. Chomski, S. Grabtchak, M. Ibisate, S. John, S. W. Leonard, C. Lopez, F. Meseguer, H. Miguez, J. P. Mondia, G. A. Ozin, O. Toader, H. M. van Driel: Nature **405**, 437 (2000)
12. K. M. Ho, C. T. Tan, C. M. Soukoulis: Phys. Rev. Lett. **65**, 3152 (1990)
13. E. Yablonovitch, T. J. Gmitter, K. M. Leung: Phys. Rev. Lett. **67**, 2295 (1991)
14. S. John: unpublished results
15. S. Noda, N. Yamamoto, M. Imada, H. Kobayashi, M. Okano: J. Lightwave Technol. **17**, 1984 (1998)
16. U. Grüning, V. Lehmann, C.M. Engelhard: Appl. Phys. Lett. **66**, 3254 (1995)
17. U. Grüning, V. Lehmann, S. Ottow, K. Busch: Appl. Phys. Lett. **68**, 747 (1996)
18. H. W. Lau, G. J. Parker, R. Greef, M. Hölling: Appl. Phys. Lett. **67**, 1877 (1995)
19. V. Lehmann, H. Föll: J. Electrochem. Soc. **137**, 653 (1990)
20. V. Lehmann, H. Föll: J. Electrochem. Soc. **140**, 2836 (1993)
21. P. Bell, J. Pendry, L. Moreno, A. Ward: Comp. Phys. Commun. **85**, 306 (1995)
22. K. Sakoda: Phys. Rev. B **52**, 7982 (1995)
23. J. Schilling, R. B. Wehrspohn, A. Birner, F. Müller, R. Hillebrand, U. Gösele, S. W. Leonard, J. P. Mondia, F. Genereux, H. M. van Driel, P. Kramper, V. Sandoghdar, K. Busch: J. Opt. A: Pure Appl. Opt. **3**, 121 (2001)

24. S. W. Leonard, H. M. van Driel, K. Busch, S. John, A. Birner, A.-P. Li, F. Müller, U. Gösele, V. Lehmann: Appl. Phys. Lett **75**, 3063 (1999)
25. J. Schilling, A. Birner, F.Müller, R. B. Wehrspohn, R. Hillebrand, U. Gösele, K. Busch, S. John, S. W. Leonard, H. M. van Driel: Opt. Mat **17**, 7 (2001)
26. S. W. Leonard, H. van Driel nad J. Schilling, R. B. Wehrspohn: Phys., Rev. B, **66**, 161102(R) (2002)
27. S. W. Leonard, J. Mondia, H. van Driel, O. Toader, S. John, K. Busch, A. Birner, U. Gösele: Phys. Rev. B **61**, R2389 (2000)
28. S. Leonard: Ph.D. Thesis, University of Toronto, Dept. of Physics (2001)
29. J. Schilling: Herstellung und optische Eigenschaften von 2D- und 3D-photonische Kristallen aus makroporösem Silizium: Ph.D. Thesis, Martin-Luther-University Halle-Wittenberg, Halle, Germany (2002)
30. S. Ottow, V. Lehmann, H. Föll: J. Electrochem. Soc., **140**, 385 (1996)
31. A. Birner: Optische Wellenleiter und Mikroresonatoren in zweidimensionalen Photonischen Kristallen aus Makroporösem Silizium: Ph.D. Thesis, Martin-Luther-University Halle-Wittenberg, Halle, Germany (2000)
32. M. Loncar, D. Nedeljkovic, T. Doll, J. Vukovich, A. Scherer, T. Pearsall: Appl. Phys. Lett. **77**, 1937 (2000)
33. A. Birner, A.-P. Li, F. Müller, U. Gösele, P. Kramper, V. Sandoghdar, J. Mlynek, K. Busch, V. Lehmann: Mat. Sci. Semicond. Proc. **3**, 487 (2000)
34. J. Schilling, F. Müller, S. Matthias, R. B. Wehrspohn, U. Gösele, K. Busch: Appl. Phys. Lett. **78**, 1180 (2001)
35. N. W. Ashcroft, N. D. Mermin: *Solid State Physics*, 2nd edn. (Springer, 1976)
36. J. Schilling, F. Müller, R. B. Wehrspohn, U. Gösele, K. Busch: Mat. Res. Soc. Symp. Proc. **722**, L6.8.1 (2002)
37. *Special issue on Photonic Crystals: Optical Materials for the 21st Century*, edited by R. B. Wehrspohn, K. Busch: Phys. Stat. Sol. A **197** (2003)
38. A. Feist, A. Lambrecht, J. Schilling, F. Müller, R. Wehrspohn: *Vorrichtung und Verfahren zur qualitativen und quantitativen Bestimmung von Gasen und Flüssigkeiten mit PBG-Struktur*, Patent DE 100 63 151 a 1

Index